Journal of the European Ceramic Society xxx (xxxx) xxx–xxx

Contents lists available at ScienceDirect

Journal of the European Ceramic Society

journal homepage: www.elsevier.com/locate/jeurceramsoc

# Cyclic ablation of high-emissivity Sm-doped $ZrB_2$/SiC coatings on alumina substrates

Anneliese E. Brenner[a], Angel A. Peña[a], Xin Li Phuah[a], Christopher Petorak[b], Brian Thompson[b], Rodney W. Trice[a,*]

[a] Purdue University, West Lafayette, IN, 47907, USA
[b] Praxair Surface Technologies Inc., Indianapolis, IN, 46222, USA

ARTICLE INFO

*Keywords:*
Hypersonic
Alumina
Samarium
Zirconium diboride
Ablation

ABSTRACT

Samarium-doped $ZrB_2$/SiC (ZBS) coatings possess properties of high emissivity and excellent ablation performance suitable for hypersonic applications. Of interest in the current study is how cyclic ablation affects the scale development on alumina substrates. ZBS coatings with 3, 5 and 8 mol% of samarium (Sm) dopant were prepared via shrouded plasma spray onto alumina substrates and subjected to two 60-s ablation cycles with temperatures reaching up to 1700 °C. Blisters were observed on the Sm-doped coatings after the 1st cycle as a result of a local eutectic reaction between the ablation products and alumina substrate. A Sm-stabilized *t*-$ZrO_2$ phase was identified through X-ray diffraction after the ablation of the Sm-doped coatings. The ZBS with 5 mol% of Sm dopant produced a flower-like microstructure after the 2nd cycle due to the formation of convection cells.

## 1. Introduction

Future hypersonic vehicle design involves the use of sharp leading edges instead of blunt ones to improve performance and reduce aerodynamic drag [1]. Increased convective heating of these edges can result in thermal shock and ablation by atmospheric friction during the reentry process [1]. Among the ultra-high temperature ceramics (UHTCs) being considered for leading edges, studies have shown that $ZrB_2$-SiC (ZBS) is one of the best materials for this application due to its high melting point and strength at 1500 °C and above, as well as its ablation and thermal shock resistance [2–4].

Studies performed by Tan et al. [3,6] have shown that adding Sm dopant to ZBS ceramics increases the emissivity compared to ceramics comprised of only ZBS. Specifically, a total hemispherical emittance of 0.9 at 1600 °C was measured for a coating comprised of 5 mol% Sm with a balance of $ZrB_2$/SiC. Furthermore, the Sm dopant improved ablation performance by forming a stable oxide scale of $c_1$-$Sm_{0.2}Zr_{0.9}O_{1.9}$, which has a melting point between 2500 °C and 2700 °C, and thus can withstand temperature extremes expected during hypersonic flight [5].

In the previous report by Tan et al. [5], a single ablation cycle of 60 s was performed on the ZBS coatings (with variable Sm concentration) applied to dense $ZrB_2$/SiC substrates. The temperature achieved was up to 2039 °C and the Sm oxide scale remain adhered to the unreacted coating. The original design of the current study was to investigate the effect of thermal cycling (e.g. repeated ablation cycles) on $ZrB_2$/SiC coatings with different levels of Sm dopant. Cyclic ablation is not well understood and it was deemed important to consider the cyclic life of these coatings when used as leading edge materials to predict of ablation resistance in dynamic environments [7]. However, the Sm-doped $ZrB_2$/SiC coatings were applied to alumina substrates rather than $ZrB_2$/SiC substrates with distinct differences in coating performance observed. Thus, in this study, ZBS coatings doped with 0, 3, 5 and 8 mol% Sm (ZBS, 3SmZBS, 5SmZBS and 8SmZBS, respectively) were evaluated via cyclic ablation testing on alumina substrates. The specimens were heated rapidly up to temperatures exceeding 1600 °C for 60 s using an oxyacetylene torch for two cycles. The microstructure and phase assemblage after each cycle were analyzed and discussed.

## 2. Experimental procedure

### 2.1. Materials and powder preparation

Spray-dried powders were prepared from a suspension that consisted of 80 vol.% $ZrB_2$ (3–5 μm, Grade A, HC Starck, Munich, Germany), 20 vol.% α-SiC (1.4 m, Grade UF-05, HC Starck, Munich, Germany), 0.4 wt.% dispersant (Darvan 821A, R.T. Vanderbilt Company, Inc., Norwalk, USA), 2 wt.% PVA binder (Celvol 203, Celanese Corporation, Dallas, USA) and DI water. The average spray-dried particle size was approximately 38 μm. Samarium dopant was

* Corresponding author at: 701 West Stadium Avenue, West Lafayette, IN, 47907, USA.
*E-mail address:* rtrice@purdue.edu (R.W. Trice).

https://doi.org/10.1016/j.jeurceramsoc.2017.11.044
Received 3 August 2017; Received in revised form 28 October 2017; Accepted 18 November 2017

added to the spray dried $ZrB_2$/SiC powders via a chemical infiltration method. In this process, 5, 10, and 15 mol% samarium nitrate hexahydrate (99.9% pure $Sm(NO_3)_3{\cdot}6H_2O$, Sigma-Aldrich, St. Louis, USA) were dissolved into 200-proof ethanol and the resulting solution was then infiltrated into the porous spray-dried $ZrB_2$/SiC powder. Next, the solvent was removed via a rotary evaporator (BM 200, Yamato Scientific America Inc., Santa Clara, USA) at 100 °C. This powder was heated at 400 °C in air for an hour to remove residual moisture and nitrates. Tan et al. [3] showed that below 400 °C both the ZBS and the Sm-doped coatings did not have any weight gain. As the normalize weight gain resulted to be approximate zero below 400 °C, it suggests that the oxygen content does not have any effect during the heat treatment at 400 °C. The first weight gain inflections start near 600 °C due to the oxidation of $ZrB_2$ to form m-$ZrO_2$ and $B_2O_3$ glass [3].

Subsequently, the dried mixture was sieved using a 60-mesh (250 µm aperture) to eliminate large agglomerates. Fumed silica (0.02 wt.%, Cab-O-Sil®, Cabot Corporation, Boston, USA) was added to all the powders as a flowing agent for feeding the powders during the plasma spray process.

The coatings were prepared at Praxair Surface Technologies (Indianapolis, USA) using a shrouded plasma spray process on alumina substrates. Table 1 shows the plasma spray deposition parameters. Powders were plasma sprayed onto 7 mm thick alumina substrates with an average coating thickness of roughly 200–350 µm. Samples were cut to 25.4 mm x 25.4 mm. The amount of Sm(NO3)3 (mol%) incorporated into the coatings was measured by mass spectroscopy on pulverized coatings (NSL Analytical Services Inc., Cleveland, USA). The actual concentrations of Sm(NO3)3 (mol%) in each coating are listed in Table 2, along with the bulk density and total porosity, measured from earlier reports [5,6]. XRD results on as-sprayed coatings showed that $ZrB_2$ is the major phase and the biggest peak of α-SiC at 35.5° (2θ). As showed on Tan results [5], a similar broad hump SmO and $Sm_2O_3$ peaks was identified on the broad hump between 26 − 35° (2θ). To help simplify discussion, the naming convention is based on the actual Sm molar concentration. For instance, the 3SmZBS coating contains ~3 mol% Sm in the $ZrB_2$/SiC matrix.

### 2.2. Oxyacetylene ablation testing

Heat flux conditions and ablation resistance were assessed using an oxyacetylene ablative torch rig. The test rig was constructed using ASTM 285-082 as a standard [6]. The ablation torch (Victor Technologies, St. Louis, USA) used a 5 mm orifice and the separation distance of 20 mm between the sample and the torch tip was held as a constant. Front and back face temperatures were measured using a two-color pyrometer (OS3750, Omega Engineering Inc., Stamford, CT, USA) which was connected to a data logger. This was used to measure temperature as a function of time. The emissivity setting for the pyrometer was estimated to be 0.9. An oxygen rich environment was simulated using an oxygen:acetylene ratio of 12:10 slpm. Test specimens were exposed to 60 s intervals of flame. Samples were cooled to room temperature and characterized before another cycle was performed. Mass change that occurred was not reported due to some of the coatings delaminating. The heat flux was measured to be 452 $W/cm^2$ using a thermogage circular foil heat flux gauge (TG1000-4, Vatell Corp., Christiansburg, VA).

**Table 1**
Plasma spray deposition parameters reproduced from reference [3].

| | |
|---|---|
| Current (A) | 200 |
| Standoff (cm) | 2.54 |
| Powder Flow (g/min) | 10 |
| Tranverse Speed (cm/s) | 117 |
| Process Gas | Argon, Hydrogen |

**Table 2**
As sprayed coating composition and properties, reproduced from [6].

| | $Sm(NO_3)_3$ (mol.%) | Actual Sm (mol.%) | Bulk Density ($g/cm^3$) | Total Porosity (%) |
|---|---|---|---|---|
| ZBS | 0 | 0 | 4.5 | 18.2 |
| 3SmZBS. | 5 | 2.8 | 4.1 | 26.1 |
| 5SmZBS | 10 | 5.3 | 3.7 | 32.0 |
| 8SmZBS | 15 | 8.2 | 3.5 | 35.7 |

### 2.3. Microstructural and phase analysis

Before performing the microstructural analysis, the samples were coated with a thin layer of Au/Pd. A scanning electron microscope (SEM) (Phillips XL-40, FEI Co., Hillsboro, USA) was used to characterize coating topography in the as sprayed conditions after each cycle. X-ray diffraction (XRD) (D8 Focus, Bruker Corporation, Billerica, USA) was used to analyze the phases present. Cu Kα radiation was used over 2θ values of 20° − 80° on the coatings after ablation using a step size of 0.02° and a scan rate of 5°/minute. Samples were aligned in the XRD to analyze the regions where the ablation flame was most intense.

## 3. Results

### 3.1. Ablation results after cycle 1

Fig. 1a shows a plot of front face temperature as a function of time during the 1st ablation cycle for each of the four coatings tested. The ZBS coating displayed a continuous temperature increase through the 60 s of heating, with a maximum of 1502 °C measured. Each of the Sm-doped coatings displayed a temperature discontinuity upon heating. This discontinuity occurred at 1570 °C, 1545 °C, and 1577 °C for the 3SmZBS, 5SmZBS, and 8SmZBS coatings after ~50s, ~40s, and ~40s, respectively. Each of the Sm-doped coatings displayed a higher front face temperature than the ZBS coating after the discontinuity.

Fig. 2 shows the surface of the coatings after the 1st ablation cycle. The ZBS coating (Fig. 2a) displayed little macroscopic evidence of the thermal cycle. Each of the Sm-doped ZBS coatings in Fig. 2b–d developed a delamination blister after the 1st cycle. Due to the limited conduction through the thickness of the coating and substrate, the blister is responsible for the increase in front face temperature and the temperature curve discontinuities observed in Fig. 1a.

The SEM micrograph of the ZBS coating after the 1st ablation cycle (Fig. 3a) shows the formation of an oxide scale with a few pores. For the Sm-doped coatings, the surface appears to have clusters of “islands” which are crystalline regions. Fig. 3b shows very fine islands in the 3SmZBS surface, while the islands in 5SmZBS in Fig. 3c appear to be larger and are surrounded by “lagoons”. Based on the micrographs in Fig. 3b–d, the islands appear to increase in size as more Sm dopant in present in the ZBS coating. Additionally, the 8SmZBS coating (Fig. 3d) has large bubbles that have burst during the ablation cycle and a crack forming.

The XRD plot for the ZBS coating in Fig. 4a match with the previous studies [3,5], where the primary phase formed was monoclinic zirconia (*m*-$ZrO_2$, JCPDS-37-1484) with very small amounts of tetragonal zirconia (*t*-$ZrO_2$, JCPDS-80-0965) observed. For the 3SmZBS, the primary phase formed is *m*-$ZrO_2$, with a Sm-stabilized *t*-$ZrO_2$ phase formed. Based on the relative intensities, the ratio of Sm-stabilized *t*-$ZrO_2$ phase to *m*-$ZrO_2$ increases as the Sm concentration increases. Only the *t*-$ZrO_2$ phase was detected for the 8SmZBS coating.

### 3.2. Ablation results after cycle 2

Fig. 1b shows the front face temperature during the 2nd 60-s ablation cycle. The maximum temperature reached by the ZBS during this

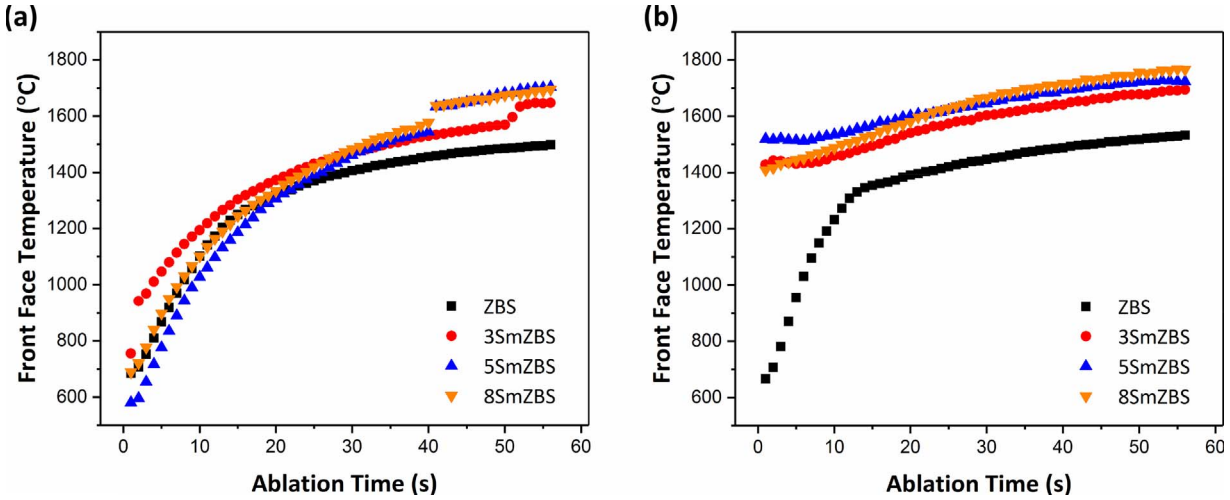


**Fig. 1.** Front face temperature during the 60-s ablation for the (a) 1st cycle and (b) 2nd cycle.

cycle reached 1540 °C, compared to 1502 °C during the 1st cycle. For the three Sm-doped coatings, the temperature curves were continuous, but significantly hotter (~200 °C) than the ZBS specimen. The increased front face temperature of the doped coatings is due to the limited conduction of heat away from front face, a consequence of the blister formed during cycle 1.

Since no temperature discontinuities were observed in Fig. 1b, there is no further blistering occurring during the 2nd ablation cycle for all the coatings. Note that the ZBS coating failed due to cracking of the underlying alumina substrate and showed little evidence of damage prior to this from ablation testing. The 3SmZBS coating (Fig. 2f) spalled off during cooling and revealed the alumina substrate below the coating. Both the 5SmZBS and 8SmZBS samples displayed a glassy layer on the surface after the 2nd ablation cycle in Figs. 2g and h. There were cracks formed on the 8SmZBS (Fig. 2h) sample upon cooling due to thermal shock.

Fig. 3e presents the surface topography of the ZBS coating after the 2nd ablation cycle; gaps have formed in the oxide scale. The islands observed in the first cycle have overall increased in sizes for the Sm-doped coatings. A similar trend as the 1st cycle is observed here, where the crystalline regions increase in size with more Sm dopant. The 5SmZBS sample surface, shown in Fig. 3g, now contains flower-like structures amongst the islands. Furthermore, the bubbles observed after cycle 1 in the 8SmZBS coating have disappeared and the microstructure now only contains the crystalline islands among the amorphous lagoon area.

Fig. 4b shows the XRD results obtained from the surface of the coatings after the 2nd ablation cycle. The XRD of ZBS remains unchanged, being mainly comprised of *m*-$ZrO_2$ with small amounts of *t*-$ZrO_2$ observed. The 3SmZBS sample had peaks associated with α-$Al_2O_3$, consistent with the spallation of the coating from the substrate as evidenced in Fig. 2f. The 5SmZBS coating was comprised of *m*-$ZrO_2$ and Sm-stabilized *t*-$ZrO_2$ phase. The 8SmZBS coating was still primarily the Sm-stabilized *t*-$ZrO_2$ phase, but peaks associated with *m*-$ZrO_2$ were observed. Both the 5SmZBS and 8SmZBS show evidence of an amorphous phase at lower 2θ.

Fig. 5 presents the SEM cross-sectional microstructure of the ZBS and 3SmZBS coating after the 2nd ablation cycle. No glassy phase is apparent at the interface where the torch was centered for the ZBS coatings (Fig. 5a, and c), and the coating remained intact with the alumina substrate. On the other hand, Sm-doped coatings separated from the substrate (Fig. 5b) and a higher magnification image (Fig. 5d)

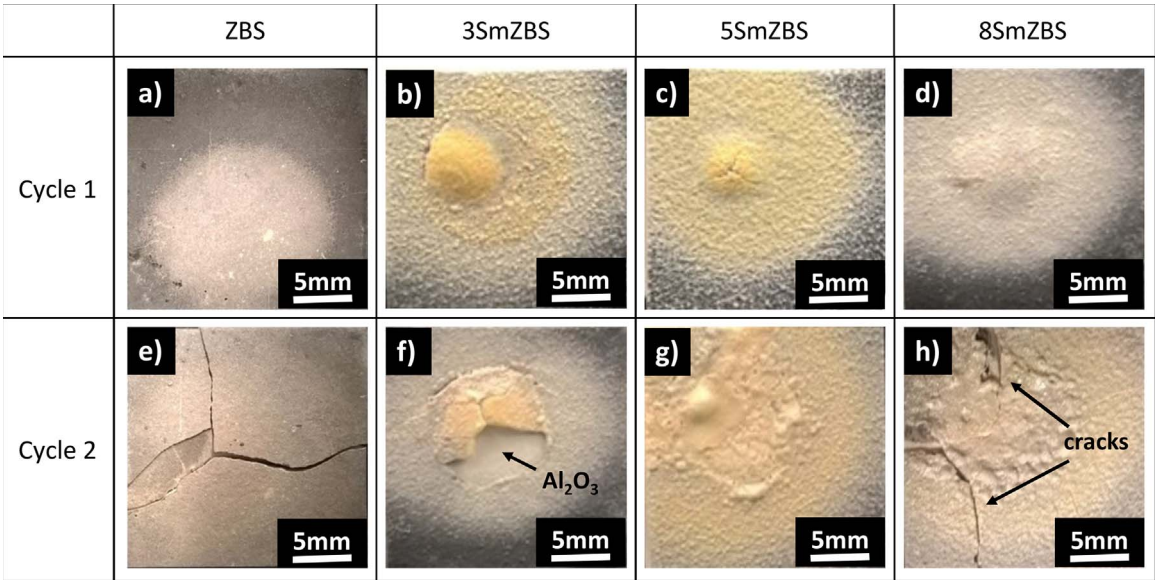


**Fig. 2.** Optical images of the ablated coatings: a) ZBS, b) 3SmZBS, c) 5SmZBS and d) 8SmZBS after cycle 1, and e) ZBS, f) 3SmZBS, g) 5SmZBS, and h) 8SmZBS after cycle 2. The $Al_2O_3$ substrate became visible in 3SmZBS after the 2nd ablation cycle due to coating delamination.

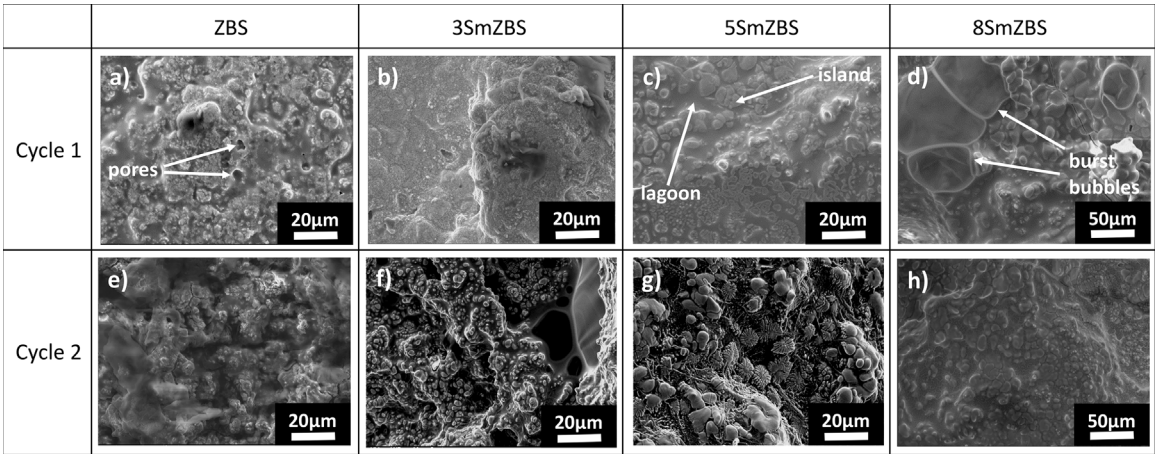


**Fig. 3.** Scanning electron micrographs of the following coatings: a) ZBS, b) 3SmZBS, c) 5SmZBS and d) 8SmZBS after cycle 1, and e) ZBS, f) 3SmZBS, g) 5SmZBS, and h) 8SmZBS after cycle 2. Burst bubbles are observed in the top right of the 8SmZBS microstructure after the 1st cycle and flower-like microstructures are observed in the 5SmZBS coating after the 2nd cycle.

revealed evidence of a glassy phase just above the blister.

## 4. Discussion

### *4.1. First observation: samarium-doped coatings blister during ablation testing*

The first observation was the blister formed in the Sm-doped ZBS coatings during ablation testing. Blister formation was not observed in the ZBS coating after either cycle 1 or 2. The $Al_2O_3/ZrO_2$ phase diagram [9], presented in Fig. 6, shows that pure $ZrO_2$ melts at 2710 °C. As $Al_2O_3$ mixes with the $ZrO_2$, there is an important eutectic reaction which occurs at 1860 °C and acts as a melting point reduction. The complete invariant reaction occurring at 1860 °C is given as:

L (58 wt.% $Al_2O_3$) $Al_2O_3$ + *t*-$ZrO_2$ (4 wt.% $Al_2O_3$)

Thus, even small amounts of alumina (> 4 wt.%) can result in a small volume percent of liquid phase. However, Fig. 1 indicates that the temperature of the coatings never reached 1860 °C during testing, and therefore, cannot be responsible for the blisters formed. For further proof that the temperature did not exceed 1860 °C, the cross sections of the ZBS coating near the alumina substrate depicted in Fig. 5a and 5c show that no residual glassy phase was observed.

A simplified ternary phase diagram showing the effect of $Sm_2O_3$ on phase assemblage when the proportions of $Al_2O_3$ and $ZrO_2$ are kept constant is presented in Fig. 7. The phase diagram shows a melting point depression at 1680 °C for an alloy with 15 mol% of $Sm_2O_3$/42.5 mol% $Al_2O_3$/42.5 mol% $ZrO_2$ that correspond to the ternary eutectic composed by $Al_2O_3$ (AL), *F*-$ZrO_2$ (F), and the perovskite structure $SmAlO_3$ (SA) [10]. The SEM cross section results for the 3SmZBS coatings revealed the presence of a glassy phase (see Fig. 5d) near the blister, indicating that the local temperature at the interface of the 3SmZBS coating and the alumina substrate exceeded 1680 °C. The composition of that glass as determined by EDS was 27 wt.% Al, 34 wt.

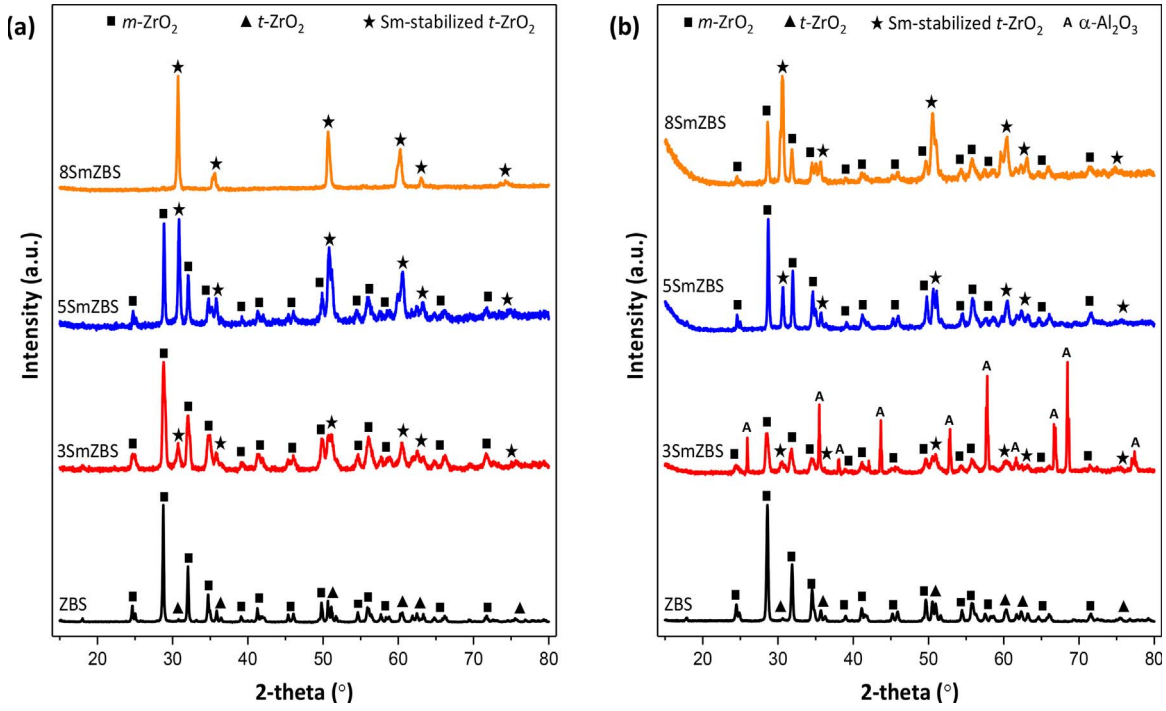


**Fig. 4.** X-ray diffraction patterns of the surface after the (a) 1st cycle and (b) 2nd cycle.

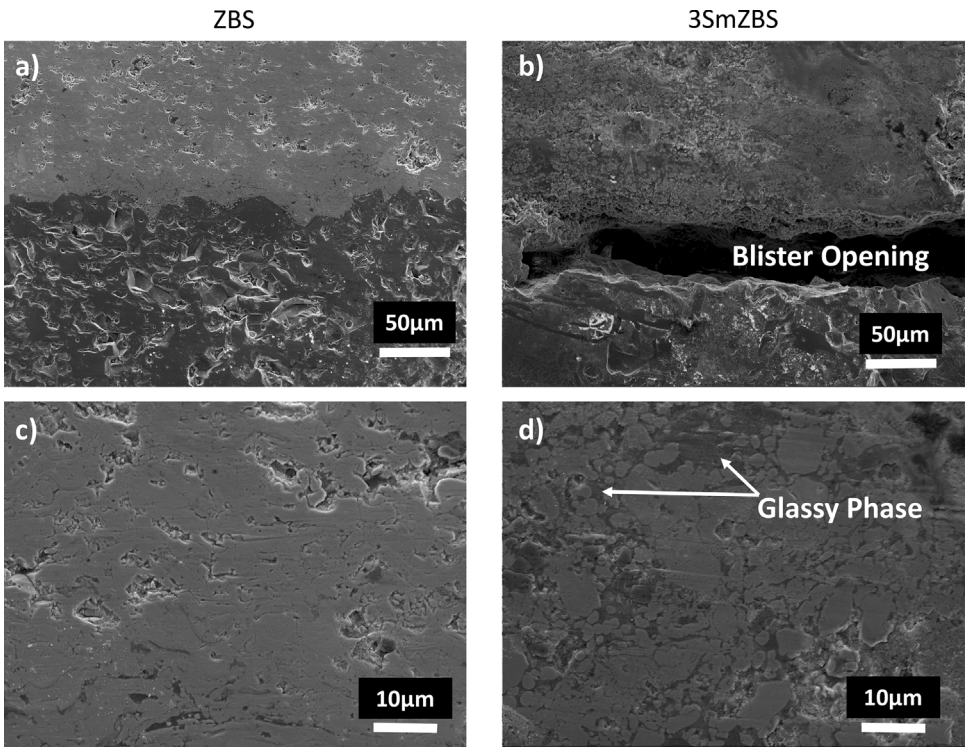


**Fig. 5.** SEM cross sections of ZBS (a) and 3SmZBS (b) at the interface between the coating and the substrate, and SEM cross sections of ZBS (c) and 3SmZBS (d) just above the interface. Glassy phase was observed in the 3SmZBS coating directly above the blister with no glassy phase observed in the ZBS coating.

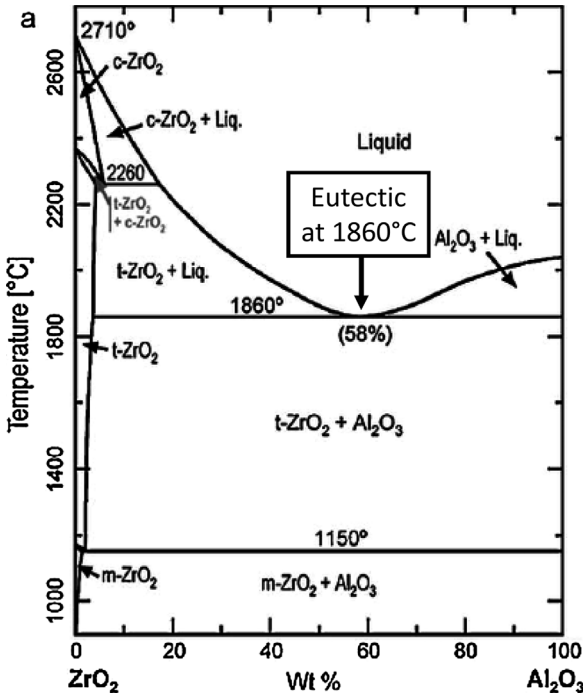


**Fig. 6.** $ZrO_2$-$Al_2O_3$ phase diagram, adapted from reference [9].

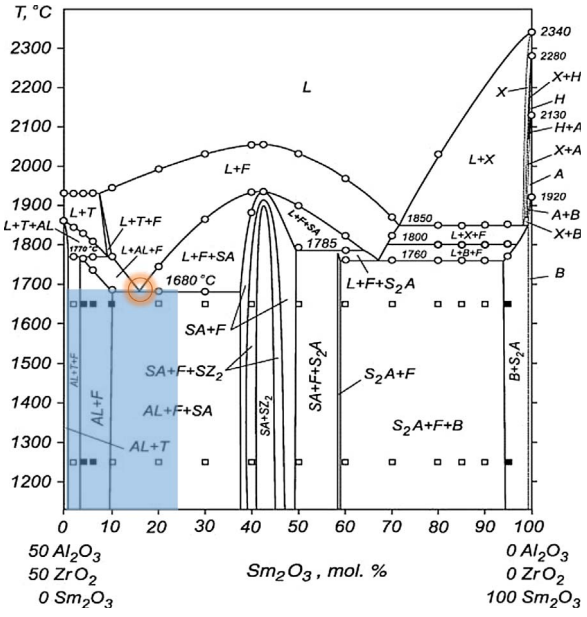


**Fig. 7.** $Al_2O_3$-$ZrO_2$-$Sm_2O_3$ phase diagram, adapted from reference [10].

% Zr, 7 wt.% Si, 27 wt.% O, and 5 wt.% Sm. The local formation of this glassy phase, centered under the hottest portions of the torch, combined with the compressive stress in the coating due to the thermal gradient through its thickness, are believed to be responsible for the formation of the blister. A similar mechanism is believed to have cause the blisters in the 5SmZBS and 8SmZBS coatings. It is also noteworthy that the blisters formed first in the 5SmZBS and 8SmZBS coatings (after ~40 s of ablation) compared to the blister formation time (~50 s) for the 3SmZBS coatings. This delay is apparent in Fig. 1a, and is consistent with the 5SmZBS and 8SmZBS coatings having more of the dopant to create the eutectic liquid.

The front face temperature of the samples during ablation were measured using a pyrometer with the emittance set at 0.9 based on prior emissivity measurements for our Sm-doped coatings tested in an inert atmosphere [6]. However, the ablation rig experiments were conducted in air, and the oxides formed likely had an emittance near 0.7 as measured by Tan et al. [5]. Based on experiments with the pyrometer, the difference between the set and actual emittance would result in the temperature measured being under estimated by 100–120 °C, approximating the difference between the measured temperature (1570 °C) and the eutectic transformation temperature (1680 °C).

### 4.2. Second observation: difference in microstructure as Sm dopant is increased

The ZBS coating demonstrated some porosity after the 1st cycle due to the evaporation of gaseous by-products, such as $B_2O_3$, CO and $CO_2$. SiC is commonly added to $ZrB_2$ in order to reduce the high evaporation rate of $B_2O_3$ by forming a silica-rich scale [11]. However, the distribution of SiC throughout the composite is discontinuous [12] and further depletion of volatile products create an uneven surface topography after the 2nd cycle as observed in Fig. 3e.

Sm is commonly used as a silica glass modifier in optical applications [13]. The addition of Sm dopant to ZBS coatings have demonstrated a reduction in viscosity of the primarily silica-based glassy phase in previous reports [3,6] and this is particularly evident for the 8SmZBS coating after cycle 1 in this study. Since the glass formed in the 8SmZBS coating had the lowest viscosity amongst the Sm-doped coatings, the evolution of volatile products can lead relatively easy bubble formation shown in Fig. 3d [14]. Bubbles are typically observed in ZBS systems between 1450 °C and 1650 °C, and they collapse and disappear within a minute during the cooling process [15]. As the glassy products are evaporated during the 1st cycle of ablation test, the overall viscosity will increase. Consequently, there were no popped bubbles observed after the 2nd ablation cycle of the 8SmZBS coating.

A flower-like microstructure was observed in Fig. 3g for the 5SmZBS coating after the 2nd cycle. Fig. 8 shows a higher magnification micrograph of the flower-like structures found at a different location. These structures were noted by Karlsdottir et al. [16] for ZBS coatings during oxidation at 1550 °C for up to 4 h. The study described the "islands" (center regions of the flower-like structure) to be *m*-$ZrO_2$, the "petals" to be $B_2O_3$ glass, and the "lagoon" regions to be $SiO_2$ glass. The formation of the flower-like structure is driven by the viscous fingering phenomena, which is the displacement of a less viscous liquid [17]. It is known that during the oxidation of ZBS coatings, $ZrB_2$ reacts to form an inner layer composed of crystalline $ZrO_2$ and liquid $B_2O_3$, and the SiC reacts to form a $SiO_2$ outer film [11,18,19]. Due to the instability of the moving interface, the less viscous $B_2O_3$ liquid displaces a more viscous $SiO_2$ liquid [19]. The rising $B_2O_3$ rich liquid contains dissolved $ZrO_2$, which deposits in the center of the flower-like structure when the $B_2O_3$ evaporates. The liquid boria-rich oxidation product is transported through the overlying layer of $SiO_2$ liquid by convection, forming convection cells aligned like the petals of a flower [16].

The flower-like structure formed on the 5SmZBS sample was not seen in the 3SmZBS and 8SmZBS coatings. Since the addition of Sm affects the viscosity of the glassy phase, this has resulted in several differences in the microstructures as a function of the amount of Sm dopant added. This is evident by the sizes of islands and lagoons in the micrographs. The low evaporation rate for 3SmZBS led to formation of very fine $ZrO_2$ islands shown after the 1st cycle (Fig. 3b). After the 2nd cycle, the islands have increased in size, similar to the island size in 5SmZBS after one cycle. For the 8SmZBS coating, the evaporation rate is much higher than the other Sm-doped coatings. The increased rate of convection cell formation will cause the $ZrO_2$ islands to impinge with each other after covering the entire surface, leaving no room for the formation of petals [20].

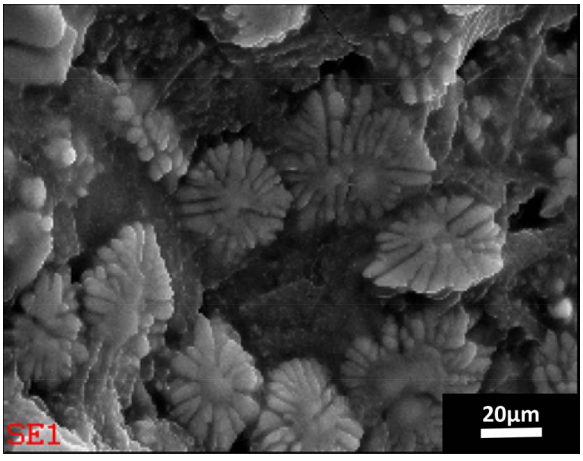


**Fig. 8.** SEM micrograph of the flower-like microstructure on the 5SmZBS coating after the 2nd cycle.

### 4.3. Third observation: formation of Sm-stabilized t-$ZrO_2$ phase

The XRD results presented in Fig. 4 showed differences in the phase assemblage on the surface of the coatings after each ablation cycle. The crystalline phases present in the ZBS sample after ablation cycles 1 and 2 remain unchanged. The primary phase found in ZBS is *m*-$ZrO_2$, with very small amounts of *t*-$ZrO_2$ detected. Some *t*-$ZrO_2$ phase remained since it was not able to transform to *m*-$ZrO_2$ during the rapid cooling process [21]. For the Sm-doped coatings, the *t*-$ZrO_2$ phase is present but at a much higher intensity. The aliovalent $Sm^{3+}$ ions stabilizes the $ZrO_2$ in a similar way $Y^{3+}$ does and can reduce the formation of *m*-$ZrO_2$ on cooling, which typically leads to cracking of the coating [8]. This can be seen with by a peak shift in the larger angle direction of 0.2θ in the XRD results presented in Fig. 4. It would be expected to see a shift in a smaller 2θ direction, however the blistering of the sample raised the ablation zone by ~1 mm, causing the shift in the opposite direction. With more Sm dopant present, it is possible to stabilize all the *t*-$ZrO_2$ phase, as demonstrated by the 8SmZBS after cycle 1. However, the limited Sm concentration was not able to further stabilize the *t*-$ZrO_2$ for the 2nd cycle, which led to the formation of *m*-$ZrO_2$. As a result, the coating evidently had formed cracks as illustrated in Fig. 2h.

The XRD results have shown that the protective oxide scales formed after ablation for the Sm-doped ZBS coatings on alumina substrates are different than those studies previously performed by Tan et al. [5] on ZBS substrates. Studies for Sm-doped ZBS coatings on ZBS substrates have shown that after ablation there are three main oxide scales formed depending on the samarium percent: *m*-$ZrO_2$, $c_1$-$Sm_{0.2}Zr_{0.9}O_{1.9}$, and $Sm_2Zr_2O_7$. Some beneficial effects of the $c_1$-$Sm_{0.2}Zr_{0.9}O_{1.9}$ oxides include their high melting point and emissivity, adherence to the unreacted coating during cooling, and formation of a dense oxide scale. Therefore, this cubic fluorite structure oxide scale provides a better ablation resistance than the *m*-$ZrO_2$ oxide scale formed on ZBS coatings. The XRD results for Sm-doped ZBS coatings on alumina substrates did not show the $c_1$-$Sm_{0.2}Zr_{0.9}O_{1.9}$ or $Sm_2Zr_2O_7$ protective oxides scales. Based on the phase diagram presented in Fig. 7, small portions of $c_1$-$Sm_{0.2}Zr_{0.9}O_{1.9}$ compound should be formed with *m*-$ZrO_2$ being the main phase. However, the temperature achieved by ablation in this report is ~400 °C lower than Tan et al.'s report [5], which may explain the different phases obtained and explain the emissivity difference. The temperature difference also explains why the presently studied coatings did not adhere to the alumina substrate.

## 5. Conclusions

Sm-doped ZBS coatings were applied by a shrouded air plasma spray onto alumina substrates and two cycles of 60-s ablation testing was performed. The phase assemblage and microstructure were evaluated after each ablation cycle. The ZBS coating did not exhibit delamination from the alumina substrate or any phase change after each cycle. The ablation of the Sm-doped coatings resulted in a blister forming after the 1st cycle due to a local eutectic reaction occurring between $Sm_2O_3$, $ZrO_2$, and $Al_2O_3$. Higher Sm concentration in the ZBS coatings lowers the viscosity of the glassy phase and increases its evaporation rate. The micrographs show that the size of $ZrO_2$ islands formed increase with more Sm added after each cycle, as the speed of forming convection cells increases. 5SmZBS coating exhibited flower-like microstructures after the 2nd ablation cycle as a result of the viscous fingering process.

The addition of Sm dopant to the ZBS forms a Sm-stabilized *t*-$ZrO_2$ phase after ablation, rather than *m*-$ZrO_2$. The addition of 8 mol% of Sm to ZBS can fully stabilize the *t*-$ZrO_2$ after a 60-s ablation cycle.

## Acknowledgement

The authors gratefully acknowledge the financial support of Dr. Ali Sayir of the Air Force Office of Scientific Research (AFOSR Grant # FA9550-16-1-0039).

## References

[1] T.H. Squire, J. Marschall, Material property requirements for analysis and design of UHTC components in hypersonic applications, J. Eur. Ceram. Soc. 30 (no. 11) (2010) 2239–2251.
[2] F. Monteverde, The thermal stability in air of hot-pressed diboride matrix composites for uses at ultra-high temperatures, Corros. Sci. 47 (no. 8) (2005) 2020–2033.
[3] W. Tan, C.A. Petorak, R.W. Trice, Rare-earth modified zirconium diboride high emissivity coatings for hypersonic applications, J. Eur. Ceram. Soc. 34 (no. 1) (2014) 1–11.
[4] M. Tului, G. Marino, T. Valente, Plasma spray deposition of ultra high temperature ceramics, Surf. Coat. Technol. 201 (no. 5) (2006) 2103–2108.
[5] W. Tan, M. Adducci, R. Trice, Evaluation of rare-earth modified $ZrB_2$- SiC ablation resistance using an oxyacetylene torch, J. Am. Ceram. Soc. 97 (no. 8) (2014) 2639–2645.
[6] W. Tan, M. Adducci, C. Petorak, A.E. Brenner, R.W. Trice, Effect of rare-earth dopant (Sm) concentration on total hemispherical emissivity and ablation resistance of $ZrB_2$/SiC coatings, J. Eur. Ceram. Soc. (2016) 1–9.
[7] L. Liu, W. Feng, X. Shi, H. Wu, J. Zhu, Effect of surface ablation products on the ablation resistance of C/C-SiC composites under oxyacetylene torch, Corros. Sci. 67 (2013) 60–66.
[8] ASTM E 285-08, Standard Test Method for Oxyacetylene Ablation Testing of Thermal Insulation Materials, ASTM International, 2008.
[9] F. Tarasi, M. Medraj, A. Dolatabadi, J. Oberste-Berghaus, C. Moreau, Amorphous and crystalline phase formation during suspension plasma spraying of the alumina-zirconia composite, J. Eur. Ceram. Soc. 31 (no. 15) (2011) 2903–2913.
[10] Lakiza, Sergij, L. Lopato, Phase diagram of the alumina?zirconia?samaria system, J. Am. Ceram. Soc. 89 (no. 11) (2006) 3516–3521.
[11] W. Fahrenholtz, 'Thermodynamic analysis of $ZrB_2$-SiC oxidation: formation of a SiC-depleted region', J. Am. Ceram. Soc. 90 (no. 1) (2007) 143–148.
[12] X. Zhang, H. Hu, C.J. Han, Structure evolution of $ZrB_2$-SiC during the oxidation in air, J. Mater. Res. 23 (no. 7) (2008) 1961–1972.
[13] M. Farries, P.R. Morkel, J.E. Townsend, Spectroscopic and lasing characteristics of samarium doped glass fibre, IEE Proc. J. (Optoelectronics) 137 (no. 5) (1990) 318–322.
[14] J. Han, P. Hu, X. Zhang, S.W. Meng Han, Oxidation-resistant $ZrB_2$-SiC compositesat 2200°C, Compos. Sci. Technol. 68 (no. 3) (2008) 799–806.
[15] S. Gangireddy, S. Karlsdottir, S. Norton, J. Tucker, J. Halloran, In situ microscopy observation of liquid flow, zirconia growth, and CO bubble formation during high temperature oxidation of zirconium diboride-silicon carbide, J. Eur. Ceram. Soc. 30 (2010) 2365–2374.
[16] S. Karlsdottir, J. Halloran, C. Henderson, Convection patterns in liquid oxide films on $ZrB_2$-SiC composites oxidized at a high temperature, J. Am. Ceram. Soc. 90 (no. 9) (2007) 2836–2867.
[17] S.J. Langer, Dendrites, viscous fingers and the theory of pattern formation, Science 243 (4895) (1989) 1150–1157.
[18] F. Monteverde, A. Bellosi, Oxidation of $ZrB_2$-based ceramics in dry air, J. Electrochem. Soc. 150 (11) (2003) 552–559.
[19] E. Opila, S. Levine, J. Lorincz, Oxidation of $ZrB_2$ and $HfB_2$-based ultra-high temperature ceramics: effect of Ta additions, J. Mater. Sci. 39 (2004) 5969–5977.
[20] S. Karlsdottir, J. Halloran, Formation of oxide films on $ZrB_2$-15 vol% SiC composites during oxidation: evolution with time and temperature, J. Am. Ceram. Soc. 6 (2009) (1328-1322).
[21] Y. Jia, H. Li, L. Feng, J. Sun, K. Li, Q. Fu, Ablation behavior of rare-earth La-modified ZrC coating for SiC-coated carbon/carbon composites under an oxyacetylene torch, Corros. Sci. 104 (2016) 61–70.